Biosensors and Bioelectronics 55 (2014) 259–265

Contents lists available at ScienceDirect

Biosensors and Bioelectronics

journal homepage: www.elsevier.com/locate/bios

A simple hydrogen peroxide biosensor based on a novel electro-magnetic poly(*p*-phenylenediamine)@Fe_3O_4 nanocomposite

Mehdi Baghayeri [a,*], Ehsan Nazarzadeh Zare [b], Moslem Mansour Lakouraj [b]

[a] Department of Chemistry, Faculty of Science, Hakim Sabzevari University, P.O. Box 397, Sabzevar, Iran
[b] Department of Organic-Polymer Chemistry, Faculty of Chemistry, University of Mazandaran, Babolsar, Iran

ARTICLE INFO

Article history:
Received 25 September 2013
Received in revised form
29 November 2013
Accepted 11 December 2013
Available online 22 December 2013

Keywords:
Poly(*p*-phenylenediamine)
Hemoglobin
Biosensor
Nanocomposite
Fe_3O_4 nanoparticles

ABSTRACT

The novel biocompatible poly(*p*-phenylenediamine) (P*p*PDA)–Fe_3O_4 nanocomposite (P*p*PDA@Fe_3O_4) was synthesized via emulsion polymerization. The P*p*PDA@Fe_3O_4 nanocomposite was characterized by Fourier transform infrared spectra (FT-IR), X-ray diffraction (XRD), field emission scanning electron microscopy (FESEM) and vibrating sample magnetometer (VSM). The P*p*PDA@Fe_3O_4 nanocomposite was then used as substrate for the immobilization of hemoglobin (Hb) and their bioelectrochemical behaviors were studied. Electrochemical impedance spectroscopy was used to confirm the adsorption of Hb onto the surface of P*p*PDA@Fe_3O_4 nanocomposite. The Hb immobilized on P*p*PDA@Fe_3O_4 nanocomposite retained its near-native conformations as characterized by the FT-IR. A pair of well-defined redox peaks of Hb was obtained at the Hb–P*p*PDA@Fe_3O_4 modified glassy carbon electrode (Hb–P*p*PDA@Fe_3O_4/GCE) through direct electron transfer between the protein and the underlying electrode. The proposed biosensor showed good reproducibility and high sensitivity to H_2O_2 with the detection limit of 0.21 μM (S/N=3). In the range of 0.5–400.0 μM, the catalytic reduction current of H_2O_2 was proportional to its concentration. The apparent Michaelis–Menten constant of Hb on the P*p*PDA@Fe_3O_4 nanocomposite was estimated to be 0.088 mM, showing its high affinity.

1. Introduction

The analytical determination of hydrogen peroxide (H_2O_2) is of great importance in many different areas, from clinical and environmental studies to industrial productions. Hydrogen peroxide (H_2O_2) is a byproduct of several highly selective oxidases, and also an essential mediator in food, biology, medicine, industry and environmental analysis (Ruzgas et al., 1996; Wang and Wang, 2004). A number of methods, such as spectrophotometry (Sunil and Narayana, 2008), fluorescence (Towne et al., 2004), and electrochemical techniques (Vianello et al., 2007; Chen et al., 2012) have been used to detect H_2O_2. With the development of sensing technology in many fields, including environment monitoring, industry and agriculture production, medical diagnosis, military and public safety, etc., electrochemical sensors play more and more important roles, due to their operational simplicity, low cost, high sensitivity and suitability for real-time detection and insensitivity to optical drawbacks, such as turbidity and quenching (Magro et al., 2013).

The current researches on H_2O_2 detection are mainly focused on electrode modifications in order to decrease the overpotential and increase the electron transfer kinetics, which will affect the sensing performance (Chen et al., 2012). A literature survey indicates that many materials have been used until now as electrode modifiers in order to minimize the overpotential of H_2O_2 oxidation or reduction (Cui et al., 2010; Salimi et al., 2013; Gligor et al., 2010; Campbell et al., 2009; Qiu et al., 2007). However, due to the high selectivity and specificity for H_2O_2, redox enzymes (horseradish peroxidase, cytochrome c, and hemoglobin)-based biosensors have been extensively employed for H_2O_2 detection (Liu et al., 2009; Rui et al., 2010; Chen et al., 2007; Guo et al., 2008). Among these redox enzymes, Hb is an ideal model enzyme because of its known structure, commercial availability, and relatively higher stability (George and Lee, 2009). On the other hand, the direct electron transfer between Hb and conventional electrodes is slow due to the deep burying of electroactive prosthetic groups as well as unfavorable orientation and/or adsorptive denaturation of Hb on the electrode surface. Therefore, to facilitate the direct electron transfer between Hb and electrode is of great importance in the development of Hb-based biosensors, but is also very challenging (Ding et al., 2010).

In recent years, magnetic nanoparticles as special bimolecular immobilizing carriers are becoming the focus of research. The use of magnetic nanoparticles as support for enzyme immobilization is endowed with the following advantages: (1) higher specific surface favors the binding efficiency, (2) lower mass transfer resistance and less fouling, (3) the selective separation of immobilized enzymes under a magnetic field and hence lower operation cost,

* Corresponding author. Tel.: +98 5714 0033 25; fax: +98 5714 0031 70.
E-mail addresses: m.baghayeri@hsu.ac.ir, mehdi.baghayeri@yahoo.com (M. Baghayeri).

0956-5663/$ - see front matter © 2014 Elsevier B.V. All rights reserved.
http://dx.doi.org/10.1016/j.bios.2013.12.033

and (4) the application of a continuous biocatalysis system (Tang et al., 2011). However, the problems of aggregation and rapid biodegradation limited applications of magnetic nanoparticles to biosensing (Peng et al., 2011). One of the most notable candidates for improvement of such practical applications may be nanomaterials based on conducting polymers. Conductive polymers have been extensively explored during the last several decades because of their excellent chemical and physical properties originating from their unique π-conjugated system (Jang et al., 2005). There has been tremendous interest in the fabrication of polymercoated nanoparticles with unique and tailored properties for various applications. These composite nanoparticles provide a robust platform for sensing application and diverse functionalities from the polymer into a single particle (Jang et al., 2006). To date, a number of methods have been described for generating organic/inorganic nanocomposites (Vestal and Zhang, 2002; Kamata et al., 2003; Caruso, 2001; Kang and Taton, 2005). One of the convenient methods for preparation of nanocomposites is emulsion polymerization. Emulsion polymerization is the most commonly used method for the production of a wide range of polymers. The use of water as the dispersion medium is environment friendly and also allows excellent heat transfer during the course of the polymerization. This technique allows particles to transfer into micelles through the surfactant template and increase the molecular weight (Prasad and Geckeler, 2011).

This work developed a simple approach for the immobilization of heme proteins by combining the advantages of super paramagnetism from Fe_3O_4 nanoparticles and conductive poly(p-phenyldiamine) (P*p*PDA) as the building block, and a novel amperometric biosensor has been developed for the determination of H_2O_2. The P*p*PDA@Fe_3O_4 nanocomposite, synthesized by a simple emulsion polymerization, was initially deposited on the glassy carbon electrode surface and then heme proteins were immobilized on the P*p*PDA@Fe_3O_4 nanocomposite surface via electrostatic interaction. The morphology and structure of nanocomposite was characterized by X-ray diffraction (XRD), field emission scanning electron microscopy (FESEM), and Fourier transform infrared spectra (FT-IR). In addition the vibrating sample magnetometer (VSM) was used for magnetization behavior of the P*p*PDA@Fe_3O_4 nanocomposite. The constructed biosensor shows excellent performance for hydrogen peroxide determination.

2. Experimental

2.1. Chemicals and reagents

p-Phenylenediamine (PpDA), ferric chloride ($FeCl_3 \cdot 6H_2O$), ferrous chloride ($FeCl_2 4H_2O$), ammonium persulfate (APS), sodium dodecyl sulfate (SDS), and all solvents were purchased from Merck (Darmstadt, Germany) and were used without further purification. Hemoglobin from bovine blood (Sigma-Aldrich) was used without further purification. Hydrogen peroxide (H_2O_2) solutions (from Sigma-Aldrich) were freshly prepared before being used. Phosphate buffer solutions (PBS) were prepared with sodium phosphate dibasic (Na_2HPO_4) and sodium monobasic (NaH_2PO_4) from Fluka. All other chemicals were of analytical grade and were used without further purification. All solutions were prepared with double-distilled water.

2.2. Preparation of Fe_3O_4 magnetic nanoparticles

Fe_3O_4 nanoparticles were synthesized following the procedure described by Cao et al. (Cao et al., 2004) as follows: 0.994 g of $FeCl_2 \cdot 4H_2O$ and 2.73 g of $FeCl_3 \cdot 6H_2O$ were dissolved in 25 ml deionized water at room temperature. The mixture was stirred mechanically at 80 °C for 15 min. and then (25%) NH_4OH (10 ml) was quickly added into the mixture until the pH reached 10. After 30 min, the black precipitate was separated by magnetic decantation and washed several times with deionized water and twice with ethanol. Finally, Fe_3O_4 magnetic nanoparticles were dried at 80 °C under vacuum for 6 h.

2.3. Synthesis of P*p*PDA@Fe_3O_4 nanocomposite

P*p*PDA@Fe_3O_4 nanocomposite were synthesized via emulsion polymerization (Scheme 1) at room temperature as follows: in a typical experiment, 0.75 g of Fe_3O_4 nanoparticles, 2.65 g SDS and 20 ml chloroform were added into 30 ml of distilled water and the mixture dispersed by an ultrasonic bath at room temperature for about 1 h. Then, the solution of *p*PDA monomer (1 g) in 30 ml of HCl (1 M) was added to the above solution. The fresh APS solution (1.5 g of APS in 20 ml deionized water) was dropped into the reaction medium for 30 min. The reaction was carried out at room temperature for 24 h. Then the reaction mixture was poured into acetone to terminate the reaction. The formed precipitate was filtered and washed with distilled water for several times and methanol for once. Finally, the obtained red dark powder was dried in vacuum at 50 °C for 24 h.

2.4. Measurements

Autolab Electrochemistry Instruments (Autolab, Eco Chemie, Netherlands) was used for amperometry measurements and electrochemical impedance spectroscopy (EIS). Cyclic voltammetry measurements were carried out on a Metrohm (797 VA Computrace, Switzerland) controlled by personal computer. A saturated

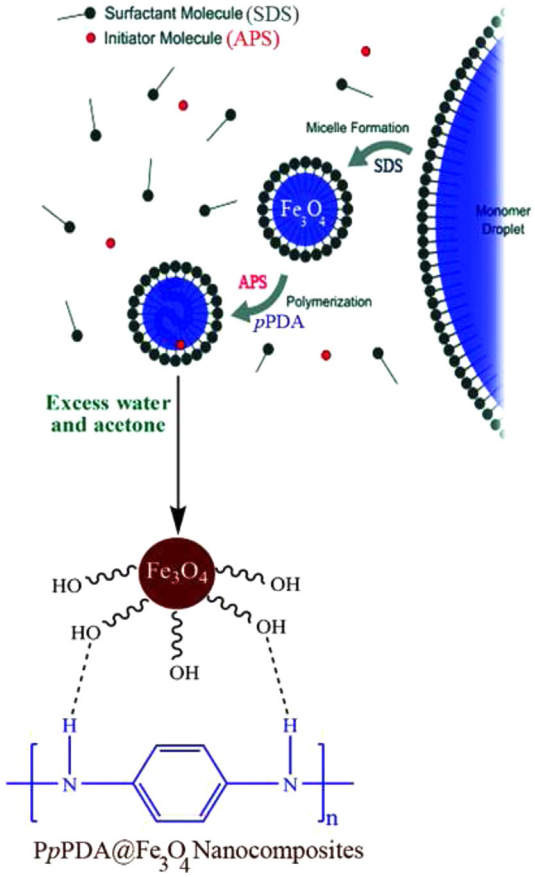

Scheme 1. Synthetic pathway of P*p*PDA@Fe_3O_4 nanocomposite.

calomel electrode (SCE) as reference electrode and a platinum wire as auxiliary electrode were used. A glassy carbon electrode, GCE, (Metrohm, Switzerland) with a geometrical area of 0.0314 cm^2, bare or modified, was used as working electrode. EIS was performed in 1.0 mM $K_3Fe(CN)_6/K_4Fe(CN)_6$ (1/1) mixture with 0.1 M KCl as supporting electrolyte, using an alternating current voltage of 5 mV, within the frequency range of 0.1–10^5 Hz.

X-ray diffraction (XRD, Rigaku Corporation, Tokyo, Japan) patterns were obtained at room temperature on a Riga kuD/Max-2550 powder diffractometer with a scanning rate of 5 min^{-1}, and recorded in the 2θ range of 10–70 °C. FESEM was recorded on a Hitachi S4160 instrument (Tokyo, Japan). VSM measurements were performed by using a Vibrating sample magnetometer (LDJ Electronics Inc., Model 9600). The magnetization measurements were carried out in an external field up to 15 kOe at room temperature. A digital pH-meter (780 pH meter, Metrohm) with precision of $\pm$0.001 was used to read the pH value of the buffer solutions. Electrolyte solutions were deoxygenated by purging pure nitrogen (99.99%) for 10 min prior to electrochemical experiments. All measurements were carried out under a nitrogen atmosphere.

2.5. Preparation of modified electrode

Prior to modification, the GCE was polished with 0.05 μm α-Al_2O_3 powder slurries until a mirror shiny surface appeared, and was sonicated sequentially in acetone, HNO_3 (1:1, v/v), NaOH (1.0 M) and ultrapure water for 3 min. Typically, 6.0 μL of the DMSO dispersion containing 1.0 mg P*p*PDA@Fe_3O_4 nanocomposite was spread evenly onto the surface of the freshly cleared GCE for preparing P*p*PDA@Fe_3O_4 film, which was allowed to dry under ambient conditions for 1 h (P*p*PDA@Fe_3O_4/GCE). Then, 8.0 μL of 20 mg/mL Hb solution (dissolved in pH 7.0 PBS) was dropped on the P*p*PDA@Fe_3O_4/GCE surface, and allowed to dry in refrigerator at 4 °C for 24 h. Finally, the Hb-immobilized electrode was rinsed throughout with 0.1 M pH 7.0 PBS to wash away the loosely adsorbed Hb molecules. The obtained electrode was labeled as Hb–P*p*PDA@Fe_3O_4/GCE. For comparison, the Hb–P*p*PDA modified glassy carbon electrode (Hb–P*p*PDA/GCE) and P*p*PDA modified glassy carbon electrode (P*p*PDA/GCE) was also prepared according to the same procedure. All the Hb-immobilized electrodes were stored at 4 °C when not in use.

3. Results and discussion

3.1. Morphological characterization of PpPDA@Fe_3O_4 nanocomposite

The structural morphology of the Fe_3O_4 nanoparticles, P*p*PDA and P*p*PDA@Fe_3O_4 nanocomposite were examined by FESEM. It is clear from Fig. 1A that the synthesized Fe_3O_4 nanoparticles are grown in large quantities and possess the nanoglobular morphology. Interestingly, it is seen that the size of nanoglobules is almost similar and possess the average diameter of 40–70 nm. The FESEM image in Fig. 1B shows that the P*p*PDA has a rod-like structure and the nanorods were separated from each other. From the high-magnification image (Fig. 1C), it can be seen that the P*p*PDA nanorods were capped with Fe_3O_4 nanoparticles. The contrast grade of the obtained P*p*PDA@Fe_3O_4 nanocomposite became much higher compared with P*p*PDA nanorods and the rodlike structure was also much clearer (Fig. 1C). Also, the FESEM image in Fig. 1C indicates that the Fe_3O_4 nanoparticles which directly attached to the surface of the P*p*PDA nanorods are nearly spherical and discrete, with relatively uniform size. Furthermore, the resulting P*p*PDA@Fe_3O_4 nanocomposite was also characterized by FT-IR and X-ray diffraction (XRD). Also, the magnetic properties of pure Fe_3O_4 nanoparticles and P*p*PDA@Fe_3O_4 nanocomposite were studied at room temperature and the results are describes in supporting data.

3.2. Spectroscopic analysis of Hb–PpPDA@Fe_3O_4 nanocomposite film

The interaction between P*p*PDA@Fe_3O_4 nanocomposite and Hb are evaluated with the FT-IR spectra of P*p*PDA, Fe_3O_4, Hb and Hb–P*p*PDA@Fe_3O_4 (Fig. 2). The spectral feature of P*p*PDA, Fe_3O_4, and P*p*PDA@Fe_3O_4 nanocomposite was well demonstrated in supporting

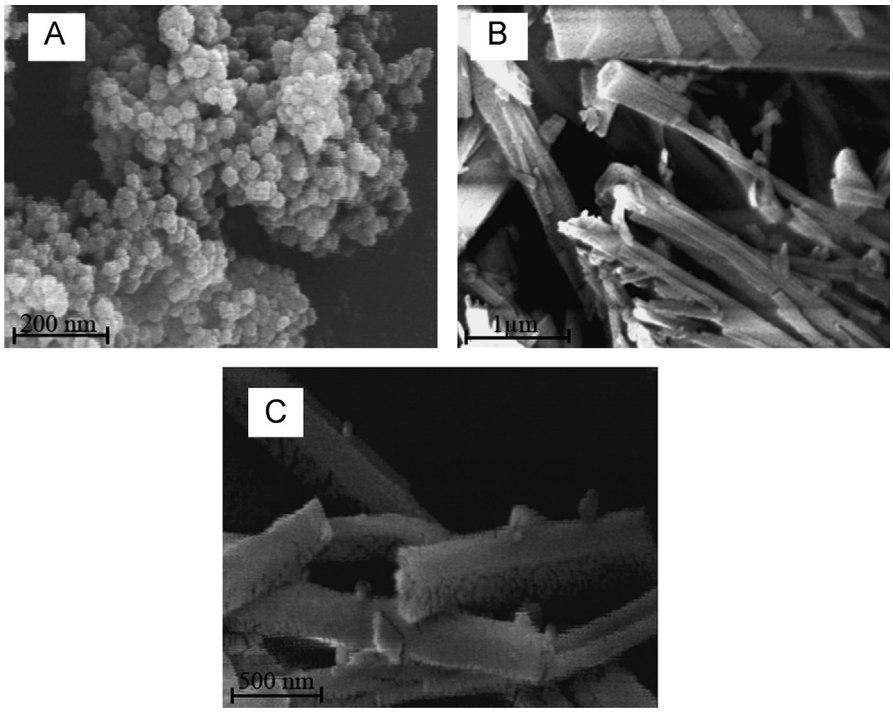

Fig. 1. FESEM micrograhs of (A) Fe_3O_4 nanoparticles, (B) P*p*PDA nanorods and (C) P*p*PDA@Fe_3O_4 nanocomposite.

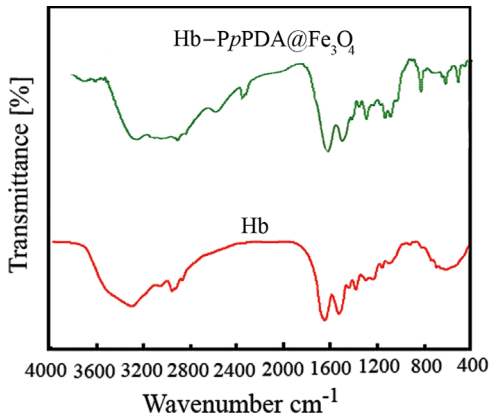

Fig. 2. FT-IR spectra of Hb and Hb–P*p*PDA@Fe_3O_4.

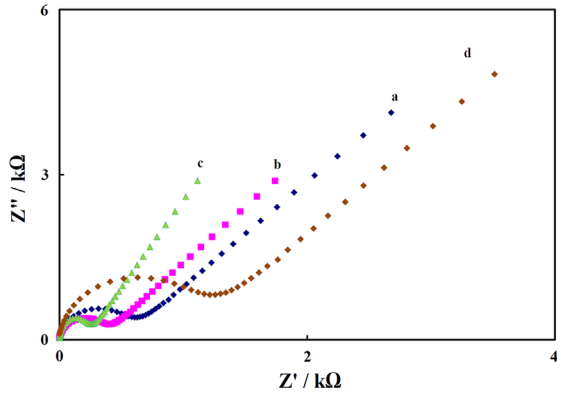

Fig. 3. Nyquist plots of (a) bare GCE, (b) P*p*PDA/GCE, (c) P*p*PDA@Fe_3O_4/GCE and (d) Hb–P*p*PDA@Fe_3O_4/GCE in 1.0 mM $K_3Fe(CN)_6$/$K_4Fe(CN)_6$ with 0.10 M KCl as the supporting electrolyte. AC amplitude: 5 mV; frequency range: 0.1–10^5 Hz.

data (Fig. S1). In FT-IR spectra of Hb, the absorbance bands at 1655 and 1543 cm^{-1} attribute mainly to the C=O stretching vibrations of the peptide linkage and combination of N–H in-plane bending and C–N stretching of the peptide groups, respectively (Baghayeri et al., 2013). The spectrum of Hb–P*p*PDA@Fe_3O_4 nanocomposite displays the combination shape of those of its components. While, the positions of the both amide bands for Hb–P*p*PDA@Fe_3O_4 are similar to those of the bare Hb; the relative intensity of the IR absorption of amide I and amide II bands seems more distinguished. Compared with the spectra of pure P*p*PDA@Fe_3O_4 and the Hb–P*p*PDA@Fe_3O_4, it should be noted that the FT-IR peaks at 1568 and 1501 cm^{-1} owing to C=N and C=C stretching vibrations of quinoid and benzenoid rings in polymer matrix that submerged with peaks in Hb. Also, the reduced intensity of the IR absorption at 3365 cm^{-1} is observed. These evidences might be due to the interaction between Hb and P*p*PDA@Fe_3O_4 (Fig. 2).

3.3. Impedance characterization of Hb–PpPDA@Fe_3O_4/GCE

EIS can provide useful information on the impedance changes of the electrode surface during the fabrication process. Fig. 3 exhibits the electrochemical impedance spectra of different modified electrodes. The electron transfer resistance (R_{et}) at the electrode surface can be used to describe the interface properties of the electrode, which is equal to the semicircle diameter of electrochemical impedance spectra (Wang et al., 2013b). The electron transfer resistance, R_{et}, derived from the semicircle domains of impedance spectra equals to 628 Ω for bare GCE (curve a). After P*p*PDA was modified on GCE (curve b), the AC impedance spectrum of the P*p*PDA/GCE showed a lower interfacial electron transfer resistance (394 Ω), indicating that the P*p*PDA film improved the electron transfer process on the surface of sensor. When the P*p*PDA@Fe_3O_4 nanocomposite was cast on the surface of the electrode (curve c), the R_{ct} was smaller (232 Ω) than that of P*p*PDA/GCE, which was attributed to the good conductivity of Fe_3O_4 nanoparticle decreased the resistance to the electrochemical reaction of $Fe(CN)_6^{3-/4-}$ couples. However, the R_{et} of Hb–P*p*PDA@-Fe_3O_4/GCE increases to 1257 Ω (curve d). It is indicated that the Hb was immobilized steadily onto the P*p*PDA@Fe_3O_4 nanocomposite. The results clearly suggest that the Hb was tightly assembled onto the P*p*PDA@Fe_3O_4 nanocomposite.

3.4. Direct electrochemistry of Hb modified electrodes

Cyclic voltammograms of different modified electrodes in pH 7.0 PBS were recorded at the scan rate of 0.1 V s^{-1} and are demonstrated in Fig. 4A. Neither P*p*PDA@Fe_3O_4/GCE (curve a) nor Hb–GCE (not shown) shows any electrochemical response in buffer solution. For Hb–P*p*PDA/GCE, a pair of small redox peaks with an anodic peak at −0.241 V and a cathodic peak at −0.411 V is observed (curve b). Compared with Hb–P*p*PDA/GCE, the peak currents at Hb–P*p*PDA@Fe_3O_4/GCE increase obviously (curve c), and a pair of well-defined redox peaks are observed. The anodic peak potential (E_{pa}) and cathodic peak potential (E_{pc}) are located at −0.281 and −0.372 V, respectively. The formal potential (defined as the midpoint of reduction and oxidation potentials), $E^{0'}$ is −0.331 V for Hb. The peak potential separation (ΔE_p, defined as $\Delta E_p = E_{pa} - E_{pc}$) is calculated as 91 mV. All of the above results revealed that the direct electron transfer between Hb and P*p*PDA@Fe_3O_4 modified GCE was greatly enhanced, and P*p*PDA@-Fe_3O_4 nanocomposite could provide a favorable microenvironment for the proteins and play an important role in improving the electron exchange.

The pH effect of supporting electrolyte on the electrochemical behaviors of Hb was explored over the range of 5.0–9.0 (Fig. 4B). Both the anodic (E_{pa}) and cathodic (E_{pc}) potential shifted negatively with the increase of pH, implying that the electrochemical process involved proton transfer. In addition, the formal potential was linearly dependent on the pH value of PBS with the slope value of 48.2 mV/pH. This slope value was smaller than the theoretical value of 57.6 mV/pH at 18 °C for a single-proton coupled reversible one-electron transfer. The reason for this difference might result from the influence of the protonation of trans and residue ligands around heme, or the protonation of the water molecule coordinated to the central iron. However, it also could indicate that a single protonation accompanies with one electron transfer of Hb Fe(III) to electrode. Then the electrochemical reduction of Hb can be simply expressed as follows: Hb heme Fe(III) $+H^+ + e^- \rightarrow$ Hb heme Fe(II) (Gao et al., 2008).

The cyclic voltammograms of the Hb–P*p*PDA@Fe_3O_4/GCE at various scan rates were measured as shown in Fig. 4C. With an increasing scan rate ranging from 0.01 to 0.4 V s^{-1}, the anodic and cathodic peak potentials of the Hb showed a small shift and the redox peak currents increased linearly, indicating a surface controlled electrode process (inset a of Fig. 4C). According to Laviron equation (Laviron, 1979a):

$$I_p = n^2F^2A\Gamma v/4RT = nFQv/4RT \quad (1)$$

where Γ is the electroactive Hb amount (mol cm^{-2}) and Q is the quantity of charge (C). The symbols n, I_p, F, R and T have their usual meanings. From the slope of the $I_p \propto v$, n was calculated to be 0.96. Therefore, the redox of Hb on P*p*PDA@Fe_3O_4 nanocomposite is a single electron transfer reaction. The average surface coverage of Hb on the surface of the modified electrode was estimated to be 2.37×10^{-9} mol cm^{-2}, which is several times larger than that of

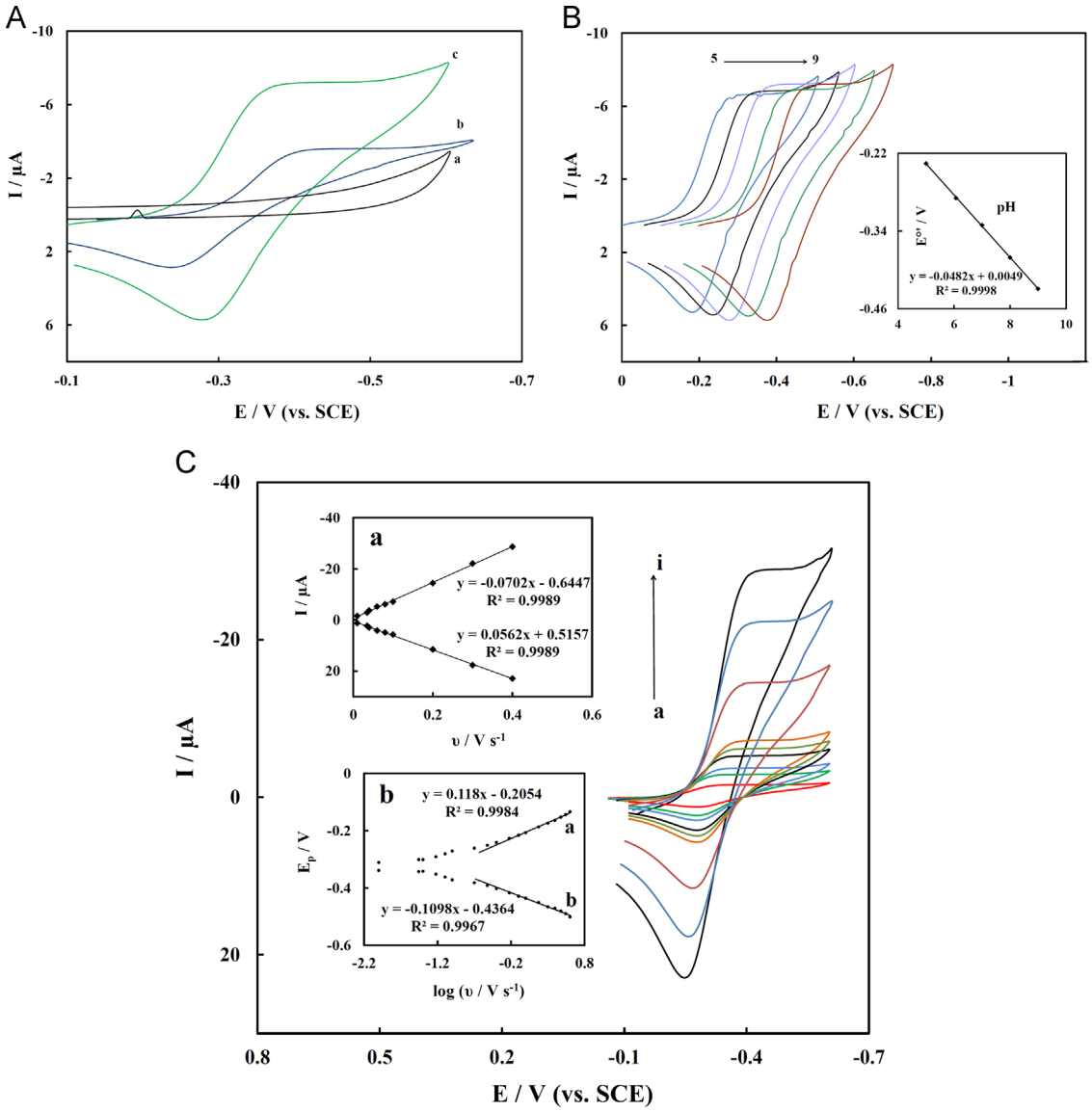

Fig. 4. (A) Cyclic voltammograms at a scan rate of 0.1 V s^{-1} in pH 7.0 PBS for (a) P*p*PDA@Fe_3O_4/GCE, (b) Hb–P*p*PDA/GCE and (c) Hb–P*p*PDA@Fe_3O_4/GCE. (B) CVs of the Hb–P*p*PDA@Fe_3O_4/GCE in 0.1 M PBS at different pH. Scan rate: 0.1 V s^{-1}. pH (from 5.0 to 9.0): 6.0, 7.0, 8.0, 9.0. Inset: plots of formal potential vs. pH. (C) CVs of Hb–P*p*PDA@Fe_3O_4/GCE in 0.1 M PBS (pH 7.0) at different scan rates of (a) 0.01, (b) 0.03, (c) 0.04, (d) 0.06, (e) 0.08, (f) 0.10, (g) 0.20, (h) 0.30 and (i) 0.40 V s^{-1}. Inset a: plot of the peak current against the scan rate. Inset b: relationship of the anodic (a) and cathodic (b) peak potential against log υ.

the theoretical monolayer coverage (1.89×10^{-11} mol cm^{-2}) (Lu et al., 2006). Electroreduction of Hb at the P*p*PDA@Fe_3O_4/GCE was also characterized by chronocoulometry. In this study, the Anson plot of charge (Q) against square root of time ($t^{1/2}$) showed a linear relationship in the presence of Hb (Anson, 1964). The surface coverage concentration (Γ^0) of analyte molecules, which were bound to P*p*PDA@Fe_3O_4 nanocomposite over the modified surface of the electrode, is calculated as 4.29×10^{-9} mol cm^{-2}. This value (4.29×10^{-9} mol cm^{-2}) confirms the value obtained by Laviron equation (2.37×10^{-9} mol cm^{-2}). This indicates that numerous layers of Hb have interacted on the surface of the electrode which implies that P*p*PDA@Fe_3O_4 nanocomposite must play a key role in promoting the direct electrochemistry of Hb in the modified electrode. The chronocoulometry results are described in supporting data.

The apparent heterogeneous electron transfer rate constant (k_s) for Hb–P*p*PDA@Fe_3O_4/GCE was estimated by cyclic voltammetry with Laviron's method (Laviron, 1979b) of the following equations:

$$E_{pc} = E^{\circ\prime} - (2.3RT/\alpha nF)\log\ \upsilon \quad (2)$$

$$E_{pa} = E^{\circ\prime} + (2.3RT/(1-\alpha)nF)\log\ \upsilon \quad (3)$$

$$\log\ k_s = \alpha\log(1-\alpha) + (1-\alpha)\log\ \alpha - \log(RT/nF\upsilon) - (1-\alpha)\alpha F\Delta E_p/2.3RT \quad (4)$$

where R is the charge transfer coefficient and n is the number of electrons transferred. The relationships of peak potentials with log υ were shown in inset b of Fig. 4C. According to Eqs. (2) and (3), the charge transfer coefficient (α) can be calculated and the result found was 0.5. The heterogeneous electron transfer rate constant (k_s) was further calculated from the relationship of ΔE_p with log υ on the basis of Eq. (4), and the result was 3.63 s^{-1}. The obtained value is superior to that of Hb immobilized Nf/nano-$CaCO_3$ film at room temperature ionic liquid modified carbon paste electrode of 0.75 s^{-1} (Sun et al., 2007), Hb immobilized on nafion modified multi-walled carbon nanotubes of 0.19 s^{-1} (Shie et al., 2009), Hb immobilized on poly(ethylene glycol) grafted multi-walled carbon nanotubes of 0.99 s^{-1} (Wen et al., 2009) and Hb in hybrid modified electrodes composed of graphene and multi-walled carbon nanotubes of 0.97 s^{-1} (Sun et al., 2013). Therefore, the

PpPDA@Fe_3O_4 nanocomposite facilitates the interfacial electron transfer between Hb heme center and the electrode surface.

The Hb–PpPDA@Fe_3O_4/GCE was stored at 4 °C, and the stability was investigated by measuring the cyclic voltammogram periodically. The results indicated that the peak potentials and currents of Hb–PpPDA@Fe_3O_4/GCE were stable for one week and then decreased gradually. Also, the cyclic voltammetric peak potentials appeared at the same position with the peak current decreasing by 20% compared with the initial response after 1 month. The reproducibility of the proposed sensor towards H_2O_2 detection was also studied. The R.S.D. of inter-electrode responses to 40 μM H_2O_2 at five different electrodes was 5.24% while the R.S.D of intra-electrode responses to five-times repeated additions of 40 μM H_2O_2 was 2.19%.

3.5. Electrocatalytic properties of Hb–PpPDA@Fe_3O_4/GCE

In order to investigate the activity of Hb at GCE modified with PpPDA@Fe_3O_4 nanocomposite, its response to the reduction of H_2O_2 was studied. Fig. S4 (Supplementary information) shows cyclic voltammograms of the modified electrode in the absence and presence of H_2O_2. When H_2O_2 was added to a pH 7.0 PBS, the reduction peak currents increased obviously accompanied by the decrease of oxidation peak current, indicating a typical electrocatalytic reduction process, which may be due to the reaction of HbFe(II) with H_2O_2. Furthermore, the reduction peak current increases with increasing concentration of H_2O_2. These results further confirmed that the PpPDA@Fe_3O_4 nanocomposite provided a friendly platform for the immobilization of Hb and the bioelectrocatalysis to H_2O_2. The electrocatalytic process can be described as follows (Zhang et al., 2011) $H_2O_2+2HbFe(II)\rightarrow 2HbFe(III)+2H_2O$

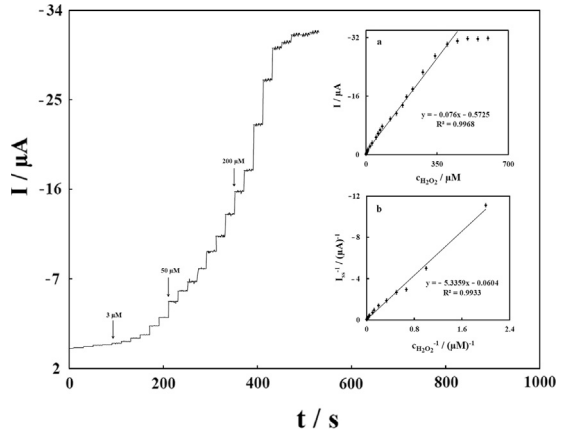

Fig. 5. Amperometric response of the H_2O_2 biosensor to successive addition of different concentration of H_2O_2 in 0.1 M PBS (pH 7.0) at the working potential of −0.4 V. Inset a: plot of electrocatalytic peak current vs. concentration of H_2O_2. Inset b: plot of the reciprocal of steady-state current (I_{ss}) vs. the reciprocal of H_2O_2 concentration for the Hb–PpPDA@Fe_3O_4/GCE.

A current–time curve at a constant potential is much more accurate and sensitive than cyclic voltammetry for the determination of current, which is usually employed to estimate a lower detection limit. Fig. 5 showed a typical steady-state amperometric response of the Hb–PpPDA@Fe_3O_4/GCE with the successive addition of H_2O_2 into the continuously stirred PBS solution at an applied potential of −0.4 V vs. SCE. Upon addition of H_2O_2, the biosensor responded rapidly to the substrates and could achieve 95% of the steady-state current within 4 s, indicating a fast amperometric response to H_2O_2 reduction.

The reduction currents increased linearly with the increasing H_2O_2 concentration (inset a of Fig. 5). The linear range was from 0.5 to 400.0 μM with a correlation coefficient of 0.9968. The detection limit was 0.21 μM (S/N=3), and the sensitivity was −0.076 μA μM^{-1}, indicating Hb immobilized in PpPDA@Fe_3O_4 nanocomposite exhibited excellent bioelectrocatalytic activity to H_2O_2. The results presented in Table 1 obviously show that the different characteristics of the proposed biosensor are better in some cases or comparable with the other biosensors reported so far. When H_2O_2 concentration was more than 400.0 μM, a response plateau in calibration curve was observed, showing the characteristics of the Michaelis–Menten kinetic mechanism (inset b of Fig. 5). The apparent Michaelis–Menten constant K_{app}^{M} provides an indication of the enzyme–substrate kinetics and a way to compare the concerned H_2O_2 sensor with others. It can be calculated from the Lineweaver–Burk equation (Li et al., 1996):

$$(1/I_{ss}) = (1/I_{max}) + (K_{app}^{M}/I_{max}C) \quad (5)$$

where I_{SS} is the steady-state current after the addition of substrate, C is the bulk concentration of the substrate, and I_{max} is the maximum current measured under saturated substrate conditions. K_{app}^{M} can be obtained by the analysis of the slope and the intercept of the plot of the reciprocals of the steady-state current vs. H_2O_2 concentration (inset b of Fig. 5). The K_{app}^{M} for the Hb–PpPDA@Fe_3O_4 modified GCE was estimated to be 0.088 mM, which is smaller than those of Hb in silica sol–gel film of 0.898 mM (Wang et al., 2004), Hb in sodium alginate–MWCNTs composite film of 0.533 mM (Zhao et al., 2009) and Hb on graphene, flower-like zinc oxide, and gold nanoparticles nanocomposite of 0.17 mM (Xie et al., 2013). This indicates that Hb immobilized on the PpPDA@-Fe_3O_4 nanocomposite exhibits a high affinity and catalytic activity to H_2O_2. In order to prove the reliability of the proposed biosensor for H_2O_2 detection, we applied the modified electrode to the determination of H_2O_2 in spiked rain water samples. The obtained results are given in Table S1. The R.S.D.% and recovery calculations indicate the potential practical application of our proposed biosensor for H_2O_2 in real samples.

Table 1
The performances of the different modified electrodes for determination of H_2O_2.

Electrode	Modifier	pH	Linear range (μM)	LOD (μM)	Reference
Glassy carbon	Poly(lactic-co-glycolic acid)/ionic liquid	7.0	5.0–8050.0	0.237	Zhang et al., 2011
Glassy carbon	Poly(acrylonitrile-*co*-acrylic acid)	7.0	9.2–2000.0	4.5	Shan et al., 2009
Glassy carbon	Poly(ε-caprolactone)	7.0	2.0–30.0	6.07	Zheng et al., 2008
Gold	Poly-allylamine	7.0	2.5–500.0	0.2	Kafi et al., 2007
Glassy carbon	PHEMA-b-DMAEMA/MWCNTs	6.0	1.0–1500.0	0.35	Wang et al., 2013b
Pyrolytic graphite	Triblock copolymer $EO_{20}PO_{70}EO_{20}$ (P123)	7.4	1–500.0	0.5	Jia et al., 2009
Glassy carbon	Poly(diallyldimethylammonium chloride)/ gold nanoparticles/graphene	7.0	6.0–1010.0	0.39	Feng et al., 2012
Gold	Chitosan@Fe_3O_4	7.0	2.3–9600.0	1.1	Wang et al., 2013a
Glassy carbon	PpPDA@Fe_3O_4	7.0	0.5–400.0	0.21	This work

4. Conclusion

A novel biocompatible P*p*PDA@Fe_3O_4 nanocomposite film has been successfully developed for the immobilization of Hb to achieve its direct electron transfer on GCE. This kind of nanocomposite film provided a favorable microenvironment around Hb to retain its biological activity and native structure. Moreover, the Hb–P*p*PDA@Fe_3O_4 modified GCE exhibited good electrocatalytical response to the reduction of H_2O_2. Therefore, P*p*PDA@Fe_3O_4 nanocomposite could offer a new promising platform for further study of the direct electrochemistry of redox proteins and the development third-generation biosensors.

Appendix A. Supporting information

Supplementary data associated with this article can be found in the online version at http://dx.doi.org/10.1016/j.bios.2013.12.033.

References

Anson, F., 1964. Anal. Chem. 36, 932–934.
Baghayeri, M., Nazarzadeh Zare, E., Namadchian, M., 2013. Sens. Actuators B: Chem. 188, 227–234.
Campbell, F.W., Belding, S.R., Baron, R., Xiao, L., Compton, R.G., 2009. J. Phys. Chem. C 113, 9053–9062.
Cao, J., Wang, Y., Yu, J., Xia, J., Zhang, C., Yin, D., Afeli, U.O.H., 2004. J. Magn. Magn. Mater. 277, 165–174.
Caruso, F., 2001. Adv. Mater. 13, 11–22.
Chen, S., Yuan, R., Chai, Y., Zhang, L., Wang, N., Li, X., 2007. Biosens. Bioelectron. 22, 1268–1274.
Chen, W., Cai, S., Ren, Q.Q., Wen, W., Zhao, Y.D., 2012. Analyst 137, 49–58.
Cui, C.-H., Li, H.-H., Yu, J.-W., Gao, M.-R., Yu, S.-H., 2010. Angew. Chem. Int. Ed. 49, 9149–9152.
Ding, Y., Wang, Y., Lei, Y., 2010. Biosens. Bioelectron. 26, 390–397.
Feng, Q., Liu, K., Fu, J., Zhang, Y., Zheng, Z., Wang, C., Du, Y., Ye, W., 2012. Electrochim. Acta 60, 304–308.
Gao, R.F., Shangguan, X.D., Qiao, G.J., Zheng, J.B., 2008. Electroanalysis 20, 2537–2542.
George, S., Lee, H.K., 2009. J. Phys. Chem. B 113, 15445–15454.
Gligor, D., Maicaneanu, A., Walcarius, A., 2010. Electrochim. Acta 55, 4050–4056.
Guo, C., Hua, F., Li, C.M., Shen, P.K., 2008. Biosens. Bioelectron. 24, 819–824.
Jang, J., Ha, J., Lim, B., 2006. Chem. Commun. 15, 1622–1624.
Jang, J., Nam, Y., Yoon, H., 2005. Adv. Mater. 17, 1382–1386.
Jia, N., Lian, Q., Wang, Z., Shen, H., 2009. Sens. Actuators B 137, 230–234.
Kafi, A.K.M., Lee, D.-Y., Park, S.-H., Kwon, Y.-S., 2007. Thin Solid Films 515, 5179–5183.
Kamata, K., Lu, Y., Xia, Y., 2003. J. Am. Chem. Soc. 125, 2384–2385.
Kang, Y., Taton, T.A., 2005. Angew. Chem. Int. Ed. 44, 409–412.
Laviron, E., 1979a. J. Electroanal. Chem. 100, 263–270.
Laviron, E., 1979b. J. Electroanal. Chem. 101, 19–28.
Li, J., Tan, S.N., Ge, H., 1996. Anal. Chim. Acta 335, 137–145.
Liu, J., Guo, C., Li, C.M., Li, Y., Chi, Q., Huang, X., Liao, L., Yu, T., 2009. Electrochem. Commun. 11, 202–205.
Lu, X.B., Hu, J.Q., Yao, X., Wang, Z.P., Li, J.H., 2006. Biomacromolecules 7, 975–980.
Magro, M., Baratella, D., Pianca, N., Toninello, A., Grancara, S., Zboril, R., Vianello, F., 2013. Sens. Actuators B: Chem. 176, 315–322.
Peng, H.-P., Liang, R.-P., Zhang, L., Qiu, J.-D., 2011. Electrochim. Acta 56, 4231–4236.
Prasad, R.J., Geckeler, K.E., 2011. Prog. Polym. Sci. 36, 887–913.
Qiu, J.D., Peng, H.Z., Liang, R.P., Li, J., Xia, X.H., 2007. Langmiur 23, 2133–2137.
Rui, Q., Komori, K., Tian, Y., Liu, H., Luo, Y., Sakai, Y., 2010. Anal. Chim. Acta 670, 57–62.
Ruzgas, T., Csöregi, E., Emneus, J., Gorton, L., 1996. Anal. Chim. Acta 330, 123–138.
Salimi, A., Rahmatpanah, R., Hallaj, R., Roushani, M., 2013. Electrochim. Acta 95, 60–70.
Shan, D., Cheng, G., Zhu, D., Xue, H., Cosnier, S., Ding, S., 2009. Sens. Actuators B: Chem. 137, 259–265.
Shie, J.-W., Yogeswaran, U., Chen, S.-M., 2009. Talanta 78, 896–902.
Sun, W., Cao, L., Deng, Y., Gong, S., Shi, F., Li, G., Sun, Z., 2013. Anal. Chim. Acta 781, 41–47.
Sun, W., Gao, R., Jiao, K., 2007. J. Phys. Chem. B 111, 4560–4567.
Sunil, K., Narayana, B., 2008. Bull. Environ. Contam. Toxicol. 81, 422–426.
Tang, T., Fan, H., Ai, S., Han, R., Qiu, Y., 2011. Chemosphere 83, 255–264.
Towne, V., Will, M., Oswald, B., Zhao, Q., 2004. Anal. Biochem. 334, 290–296.
Vestal, C.R., Zhang, Z.J., 2002. J. Am. Chem. Soc. 124, 14312–14313.
Vianello, F., Zennaro, L., Rigo, A., 2007. Biosens. Bioelectron. 22, 2694–2699.
Wang, L., Wang, E., 2004. Electrochem. Commun. 6, 225–229.
Wang, Q.L., Lu, G.X., Yang, B.J., 2004. Sens. Actuators B: Chem. 99, 50–57.
Wang, Y.-H., Yu, C.-M., Pan, Z.-Q., Wang, Y.-F., Guo, J.-W., Gu, H.-Y., 2013a. Microchim. Acta 180, 659–667.
Wang, Z., Yia, J., Yang, S., 2013b. Sens. Actuators B: Chem. 176, 211–216.
Wen, Y., Wu, H., Chen, S., Lu, Y., Shen, H., Jia, N., 2009. Electrochim. Acta 54, 7078–7084.
Zhang, Y., Sun, X., Jia, N., 2011. Sens. Actuators B: Chem. 157, 527–532.
Zhao, H.Y., Zheng, W., Meng, Z.X., Zhou, H.M., Xu, X.X., Li, Z., Zheng, Y.F., 2009. Biosens. Bioelectron. 24, 2352–2357.
Zheng, W., Li, J., Zheng, Y.F., 2008. Biosens. Bioelectron. 23, 1562–1566.
Xie, L., Xu, Y., Cao, X., 2013. Colloids Surf. B 107, 245–250.